

# The Red Giant Branch in Near-Infrared Colour-Magnitude Diagrams. II: The luminosity of the Bump and the Tip <sup>\*</sup>

E. Valenti<sup>1,2</sup>, F. R. Ferraro<sup>1</sup>, L. Origlia<sup>2</sup>

<sup>1</sup> *Dipartimento Astronomia, Università di Bologna, Via Ranzani 1, I-40127 Bologna, Italy, e-mail elena.valenti2@studio.unibo.it, ferraro@bo.astro.it*

<sup>2</sup> *INAF-Osservatorio Astronomico di Bologna, Via Ranzani 1, I-40127 Bologna, Italy, e-mail origlia@bo.astro.it*

23 October 2018

## ABSTRACT

We present new empirical calibrations of the Red Giant Branch (RGB) Bump and Tip based on a homogeneous near-Infrared database of 24 Galactic Globular Clusters. The luminosities of the RGB Bump and Tip in the J, H and K bands and their dependence on the cluster metallicity have been studied, yielding empirical relationships. By using recent transformations between the observational and theoretical planes, we also derived similar calibrations in terms of bolometric luminosity. Direct comparison between updated theoretical models and observations show an excellent agreement. The empirical calibration of the RGB Tip luminosity in the near-Infrared passbands presented here is a fundamental tool to derive distances to far galaxies beyond the Local Group, in view of using the new ground-based adaptive optics facilities and, in the next future, the James Webb Space Telescope.

**Key words:**

## 1 INTRODUCTION

This is the second in a series of papers aimed at studying the Red Giant Branch (RGB) photometric properties and its major evolutionary features in the near-Infrared (IR) spectral domain. In the first paper (Valenti et al. 2004b, hereafter Paper I) an extensive database, collected by our group over the last 10 years, has been presented. By combining a new sample of 10 Galactic Globular Clusters (GGCs) belonging to different galactic populations (i.e. Halo and Bulge) with the data set published by Ferraro et al. (2000, hereafter F00), Valenti et al. (2004a) and Sollima et al. (2004, hereafter S04), a homogeneous sample of 24 GGCs spanning a wide metallicity range ( $-2.12 \leq [\text{Fe}/\text{H}] \leq -0.49$ ) has been obtained (see Table 1). In Paper I, the entire database, calibrated in the *Two Micron All Sky Survey* (2MASS) photometric system, has been used to measure a set of photometric indices describing the RGB: *i*) location (colours and magnitudes), and *ii*) morphology (slope). Updated calibrations of these indices in terms of the clusters metallicity have been also derived. More details on the dataset can be found in Paper I.

In the present paper the major RGB evolutionary features,

namely the Bump and the Tip, are measured in the J, H and K bands. Their calibrations as a function of the clusters metallicity, in both the observational and theoretical planes, are derived and discussed.

The RGB Tip luminosity is a bright standard candle and turns to be particularly useful to measure galaxy distances. The extension of the RGB Tip calibrations to the near-IR passbands is of fundamental importance since the recent advent of ground-based adaptive optics systems and the future availability of the James Webb Space Telescope are allowing to spatially resolve bright giants and to accurately measure their magnitudes up to a few Mpc distances.

In §2 and § we measure the near-IR magnitudes of the RGB Bump and Tip, respectively, of our sample of 24 GGCs and we investigate their behaviour with varying the cluster metallicity. The results of the transformations between the observational and theoretical planes for the RGB Bump and Tip luminosities are presented in §4. Finally, in §5 we briefly summarize our results.

## 2 THE RGB BUMP

Theoretical models of stellar evolution predict that at some level along the RGB, the convective envelope penetrates deep enough into the star to reach the region of varying hydrogen abundance settled during the core hydrogen-burning.

<sup>\*</sup> Based on data taken at the ESO-MPI 2.2m Telescope equipped with the near-IR camera IRAC2-ESO, La Silla (Chile).

**Table 1.** Adopted parameters for the program clusters.

| Cluster      | [Fe/H] <sub>CG97</sub> | [M/H]        | E(B-V) | (m-M) <sub>0</sub> |
|--------------|------------------------|--------------|--------|--------------------|
| M 92         | -2.16                  | -1.95        | 0.02   | 14.78              |
| M 15         | -2.12                  | -1.91        | 0.09   | 15.15              |
| M 68         | -1.99                  | -1.81        | 0.04   | 15.14              |
| M 30         | -1.91                  | -1.71        | 0.03   | 14.71              |
| M 55         | -1.61                  | -1.41        | 0.07   | 13.82              |
| $\omega$ Cen | -1.60                  | -1.39        | 0.11   | 13.70              |
| NGC 6752     | -1.42                  | -1.21        | 0.04   | 13.18              |
| M 10         | -1.41                  | -1.25        | 0.28   | 13.38              |
| M 13         | -1.39                  | -1.18        | 0.02   | 14.43              |
| M 3          | -1.34                  | -1.16        | 0.01   | 15.03              |
| M 4          | -1.19                  | -0.94        | 0.36   | 11.68              |
| NGC 362      | -1.15                  | -0.99        | 0.05   | 14.68              |
| M 5          | -1.11                  | -0.90        | 0.03   | 14.37              |
| NGC 288      | -1.07                  | -0.85        | 0.03   | 14.73              |
| M 107        | -0.87                  | -0.70        | 0.33   | 13.95              |
| NGC 6380     | -0.87                  | -0.68        | 1.29   | 14.81              |
| NGC 6342     | -0.71                  | -0.53        | 0.57   | 14.63              |
| 47 Tuc       | -0.70                  | -0.59        | 0.04   | 13.32              |
| M 69         | -0.68                  | -0.55        | 0.17   | 14.64              |
| NGC 6441     | -0.68                  | -0.52        | 0.52   | 15.65              |
| NGC 6624     | -0.63                  | -0.48        | 0.28   | 14.63              |
| NGC 6440     | -0.49                  | -0.40        | 1.15   | 14.58              |
| NGC 6553     | -0.44;-0.06*           | -0.36;-0.05* | 0.84   | 13.46              |
| NGC 6528     | -0.38;+0.07*           | -0.31;+0.05* | 0.62   | 14.37              |

(\*) The most recent metallicity estimate by means of high resolution spectroscopy from Carretta et al. (2001).

When the convective envelope retreats from the advancing H-burning shell, a discontinuity in the H abundance profile (X) is left. Thus, the advancing H-burning shell (*i*) passes through the discontinuity and (*ii*) moves from a region of increasing X to a region of constant X. Event (*i*) generates a temporary drop in luminosity during the evolution of the star along the RGB: from an observational point of view this evolutionary hesitation yields to a peak in the differential luminosity function (LF). Event (*ii*) produces a change in the evolutionary rate of the star along the RGB, hence a change of the integrated LF slope. Crocker & Rood (1990) have made an extensive study of the best observable to locate the RGB Bump, concluding that the integrated LF is a suitable tool to reliably locate it.

Fusi Pecci et al. (1990) and more recently Ferraro et al. (1999), F00, Zoccali et al. (1999, 2000); Cho & Lee (2002); Riello et al. (2003); Valenti et al. (2004a) and S04 showed how this feature can be safely identified in most of the current generation of optical and IR CMDs of GGCs, and also in other stellar systems (see e.g Bellazzini et al. 2001b, 2002; Monaco et al. 2002). Basically, the main difficulty in detecting the RGB Bump is represented by the necessity of a large observed sample of RGB stars. This becomes particularly difficult in the case of low-metallicity GGCs, where the Bump occurs in the brightest portion of the RGB, which is an intrinsically poorly populated sequence, due to the high-evolutionary rate of stars at the very end of the RGB

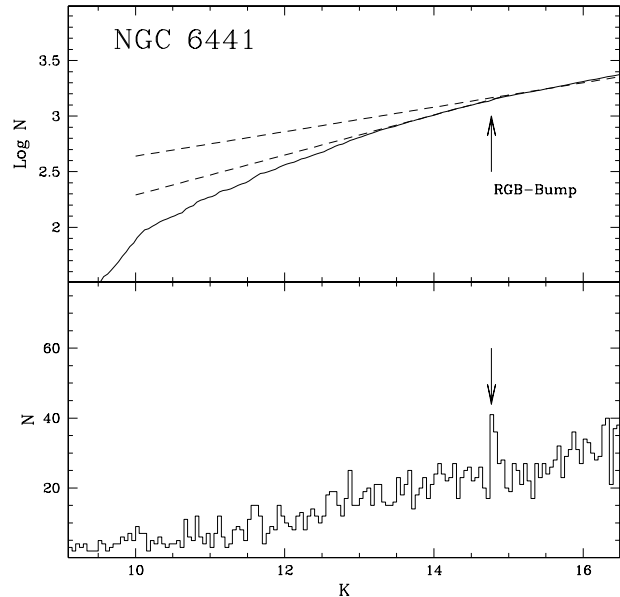


**Figure 1.** Observed integrated (upper panel) and differential (lower panel) luminosity function for RGB stars in NGC 6441. The dashed lines in the upper panel are the linear fits to the region above and below the RGB Bump.

stage. Following the same procedure as in F00 we identified the RGB Bump in most of the clusters in our sample and in all the available photometric bands, by using both the differential and integrated LFs. As an example, Fig. 1 shows both the LFs for the metal rich cluster NGC 6441. In the case of M 30, our sample is not sufficiently large to reach a safely detection of the Bump. In order to increase the fraction of the sampled cluster population, complementary data from the 2MASS catalog have been also used. The RGB Bump identified from our data was re-computed on the combined catalog. The inferred Bump K-magnitude values can be transformed into V-magnitudes by using the (V-K)<sub>0</sub> colours. The derived values are fully consistent with the direct determination of the Bump V-magnitudes listed in Tab. 5 of Ferraro et al. (1999).

The observed values of the RGB Bump for the global cluster sample are listed in Table 2. By adopting the reddening and distance moduli listed in Table 1 these values were converted into absolute magnitudes and their behaviour with varying the metallicity in the Carretta & Gratton (1997, hereafter GC97) ([Fe/H]<sub>CG97</sub>) and in the global ([M/H]) scale defined by Ferraro et al. (1999) have been shown in Figs. 2 and 3. By using 2MASS data, Cho & Lee (2002) determined the M<sub>K</sub> Bump for 11 GGCs, 7 in common with our sample, spanning a quite large metallicity range. Their estimates are in nice agreement with those of this work, F00, Valenti et al. (2004a) and S04. In order to derive a more robust relation between the absolute M<sub>K</sub> magnitude and the metallicity, the best-fitting relation has been obtained by using also the Cho & Lee (2002) data. The comparison between the observational data and the theoretical predictions based on the Straniero et al. (1997, hereafter SCL97) models, shows an excellent agreement. The inferred

**Table 2.** Near-IR and Bolometric RGB Bump magnitudes for the observed clusters.

| Name                 | [Fe/H] <sub>CG97</sub> | [M/H] | J          | H          | K          | M <sub>Bol</sub> |
|----------------------|------------------------|-------|------------|------------|------------|------------------|
| M 92                 | -2.16                  | -1.95 | 12.85±0.05 | –          | 12.35±0.05 | -0.52±0.21       |
| M 15                 | -2.12                  | -1.91 | 13.55±0.05 | 13.05±0.05 | 12.95±0.05 | -0.29±0.21       |
| M 68                 | -1.99                  | -1.81 | 13.35±0.05 | –          | 12.80±0.05 | -0.41±0.21       |
| M 30                 | -1.91                  | -1.71 | –          | –          | –          | –                |
| M 55                 | -1.61                  | -1.41 | 12.35±0.05 | –          | 11.75±0.05 | -0.17±0.21       |
| ω Cen <sup>(a)</sup> | -1.60                  | -1.39 | 12.40±0.05 | –          | 11.80±0.05 | -0.02±0.22       |
| NGC 6752             | -1.42                  | -1.21 | 11.90±0.05 | 11.35±0.05 | 11.25±0.05 | 0.08±0.21        |
| M 10                 | -1.41                  | -1.25 | –          | –          | –          | –                |
| M 13                 | -1.39                  | -1.18 | 13.05±0.05 | –          | 12.40±0.05 | 0.02±0.21        |
| M 3                  | -1.34                  | -1.16 | 13.70±0.05 | –          | 13.10±0.05 | 0.13±0.21        |
| M 4                  | -1.19                  | -0.94 | –          | –          | –          | –                |
| NGC 362              | -1.15                  | -0.99 | 13.80±0.05 | 13.25±0.05 | 13.15±0.05 | 0.53±0.21        |
| M 5                  | -1.11                  | -0.90 | 13.25±0.05 | –          | 12.65±0.05 | 0.33±0.21        |
| NGC 288              | -1.07                  | -0.85 | 13.75±0.05 | 13.25±0.05 | 13.20±0.05 | 0.51±0.21        |
| M 107                | -0.87                  | -0.70 | 13.25±0.05 | –          | 12.50±0.05 | 0.45±0.21        |
| NGC 6380             | -0.87                  | -0.68 | 15.15±0.05 | 14.25±0.05 | 13.95±0.05 | 0.64±0.22        |
| NGC 6342             | -0.71                  | -0.53 | 14.65±0.10 | 13.85±0.10 | 13.75±0.10 | 0.97±0.22        |
| 47 Tuc               | -0.70                  | -0.59 | 12.65±0.05 | 12.15±0.05 | 12.05±0.05 | 0.79±0.21        |
| M 69                 | -0.68                  | -0.55 | 14.25±0.05 | –          | 13.53±0.05 | 0.88±0.21        |
| NGC 6441             | -0.68                  | -0.52 | 15.70±0.05 | 14.85±0.05 | 14.77±0.05 | 0.95±0.22        |
| NGC 6624             | -0.63                  | -0.48 | 14.45±0.05 | 13.60±0.05 | 13.65±0.05 | 1.02±0.22        |
| NGC 6440             | -0.49                  | -0.40 | 15.30±0.05 | 14.35±0.05 | 14.13±0.05 | 1.21±0.22        |
| NGC 6553             | -0.44                  | -0.36 | 14.05±0.1  | –          | 13.05±0.10 | 1.32±0.22        |
| NGC 6528             | -0.38                  | -0.31 | 15.10±0.1  | –          | 14.05±0.10 | 1.54±0.22        |

(a) The observed RGB Bump magnitudes are from S04.

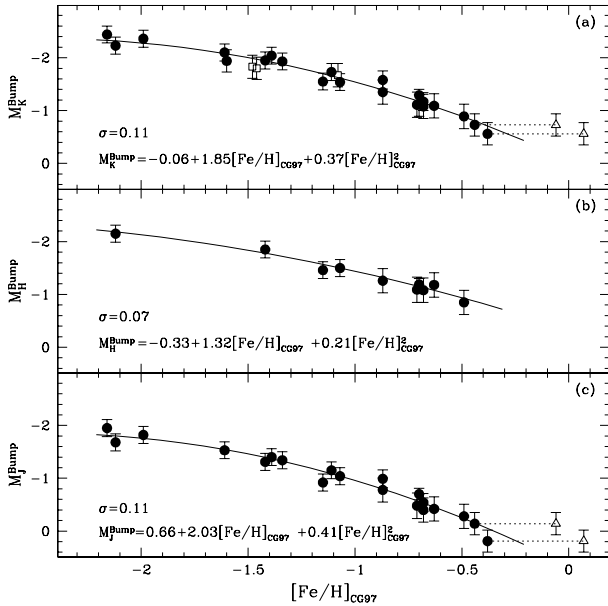


**Figure 2.** RGB Bump absolute K (a), H (b) and J (c) magnitudes as a function of the cluster metallicity in the CG97 scale. Filled circles: program clusters; empty squares: clusters in the Cho & Lee (2002) dataset; empty triangles: NGC 6553 and NGC 6528 with the most recent metallicity estimates from Carretta et al. (2001). Solid lines are our best-fitting relations to the data.

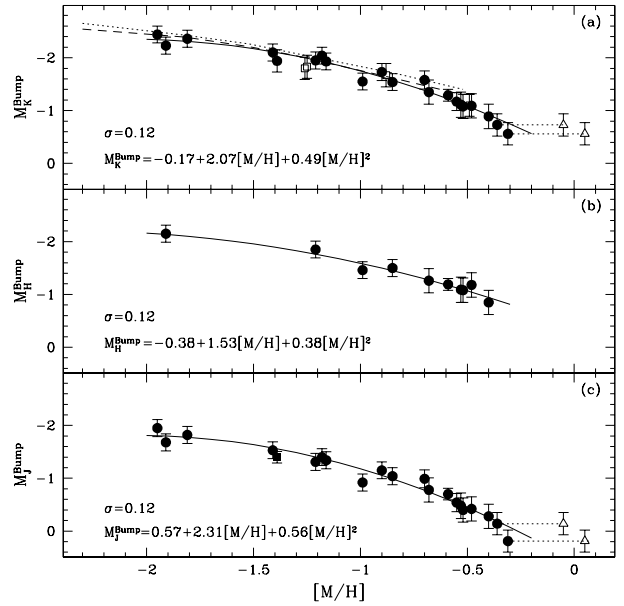


**Figure 3.** RGB Bump absolute K (a), H (b) and J (c) magnitudes as a function of the cluster metallicity in the global metallicity scale ([M/H]). Notation as in Fig. 2. Solid lines are our best-fitting relations to the data. The dotted and dashed lines in panel (a) are the theoretical predictions by SCL97 models at  $t=12$  and  $14$  Gyr.

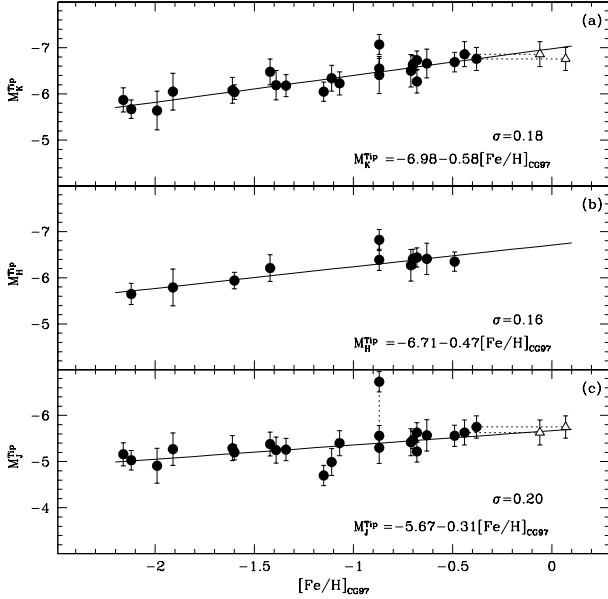


**Figure 4.** J, H and K absolute magnitude of the RGB Tip as a function of the metallicity in the CG97 scale for the entire clusters sample. The empty triangles refer to NGC 6553 and NGC 6528 with the most recent metallicity estimates by Carretta et al. (2001). Two points (filled circles) have been plotted for NGC 6380 (see §4.6 for the discussion) and connected by a dotted line. The solid lines are our best-fitting relations.

best-fitting relations to the observed points (also reported in each panel of Figs. 2 and 3 with the corresponding standard deviation) are as follows:

$$M_J^{Bump} = 0.66 + 2.03[Fe/H]_{CG97} + 0.41[Fe/H]_{CG97}^2 \quad (1)$$

$$M_H^{Bump} = -0.33 + 1.32[Fe/H]_{CG97} + 0.21[Fe/H]_{CG97}^2 \quad (2)$$

$$M_K^{Bump} = -0.08 + 1.82[Fe/H]_{CG97} + 0.36[Fe/H]_{CG97}^2 \quad (3)$$

$$M_J^{Bump} = 0.57 + 2.31[M/H] + 0.56[M/H]^2 \quad (4)$$

$$M_H^{Bump} = -0.38 + 1.53[M/H] + 0.38[M/H]^2 \quad (5)$$

$$M_K^{Bump} = -0.17 + 2.07[M/H] + 0.49[M/H]^2 \quad (6)$$

### 3 THE RGB TIP

The evolution along the RGB ends at the so-called RGB Tip with the helium-ignition in the stellar core. In globular cluster stars this event is moderately violent (the so-called helium-flash) because it takes place in a electron-degenerate core. The luminosity of the RGB Tip is a quantity well predicted by the theoretical models and, in recent years it has been widely used as a standard candle to estimate distance to various stellar systems. In fact, the RGB reaches its maximum extension in luminosity, for stellar populations older than  $\tau \approx 1 - 2$  Gyr (i.e. when stars less massive than  $M \approx 2.0 M_\odot$  are evolving) and it remains approximately constant increasing the age of the population. For this reason the method can be (in principle) successfully applied to a

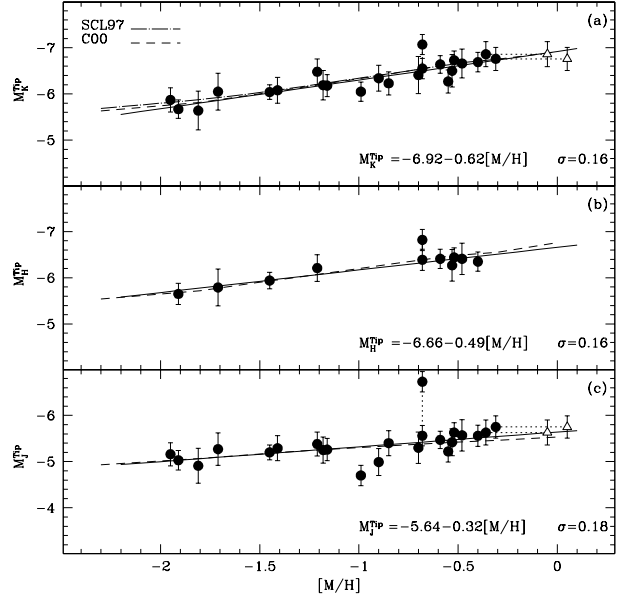


**Figure 5.** J, H and K absolute magnitude of the RGB Tip as a function of the global metallicity scale for the program clusters. estimates by Carretta et al. (2001). Notation as in Fig. 4. The solid lines are our best-fitting relations, the dashed lines are the theoretical predictions by C00 and the dot-dashed line is the SCL97 model.

variety of galaxies where a significant fraction of the population be sufficiently old to have developed the full extension of the RGB. GGCs are the best template simple stellar populations where the RGB luminosity can be empirically calibrated as a function of metallicity. In this framework our group is currently performing accurate empirical calibrations of the RGB Tip luminosity in various photometric passbands, in order to increase the potentiality and the applicability of this method to the definition of the distance scale.

Here we present a new calibration of the RGB Tip magnitudes with varying metallicity in the near-IR J, H and K bands. We adopt the method used in previous papers (see F00 and Valenti et al. 2004a), by assuming the brightest non-variable star as representative of the RGB Tip level. Obviously, particular care was payed to decontaminate the sample from background field stars and, more crucial, from the presence of Asymptotic Giant Branch (AGB) stars, which however, are significantly less numerous than RGB stars, given their much faster evolutionary rate. Moreover in low-intermediate metallicity clusters no long-period AGB stars are expected.

The observed J, H and K magnitudes of the RGB Tip for the global sample are listed in Table 3. Fig. 4 and 5 show the absolute RGB Tip magnitudes a function of the cluster metallicity in both the adopted scales. Two points have been plotted for NGC 6380. As discussed in Paper I, its RGB shape and its well-defined HB clump suggest a metallicity higher than 47 Tuc, thus it is expected to have several bright variable AGB stars populating the upper part of the RGB, but none of them have been identified yet and a clear discrimination was not possible. Hence, since the brightest

**Table 3.** Observed and Bolometric RGB Tip magnitudes.

| Name                    | [Fe/H] <sub>CG97</sub> | [M/H] | J          | H         | K         | M <sub>Bol</sub> |
|-------------------------|------------------------|-------|------------|-----------|-----------|------------------|
| M 92                    | -2.16                  | -1.95 | 9.64±0.25  | –         | 8.92±0.26 | -3.64±0.26       |
| M 15                    | -2.12                  | -1.91 | 10.20±0.21 | 9.55±0.23 | 9.42±0.20 | -3.55±0.20       |
| M 68                    | -1.99                  | -1.81 | 10.26±0.38 | –         | 9.51±0.40 | -3.37±0.40       |
| M 30                    | -1.91                  | -1.71 | 9.45±0.29  | 8.94±0.35 | 8.67±0.35 | -3.70±0.35       |
| M 55                    | -1.61                  | -1.41 | 8.59±0.27  | –         | 7.77±0.28 | -3.71±0.28       |
| ω Cen <sup>(a)</sup>    | -1.60                  | -1.39 | 8.59±0.06  | 7.81±0.08 | 7.70±0.06 | -3.59±0.16       |
| NGC 6752 <sup>(b)</sup> | -1.42                  | -1.21 | 7.84±0.25  | 6.99±0.25 | 6.72±0.28 | -3.65±0.28       |
| M 10                    | -1.41                  | -1.25 | –          | –         | –         | –                |
| M 13                    | -1.39                  | -1.18 | 9.20±0.28  | –         | 8.25±0.32 | -3.59±0.32       |
| M 3                     | -1.34                  | -1.16 | 9.78±0.24  | –         | 8.85±0.24 | -3.61±0.24       |
| M 4                     | -1.19                  | -0.94 | –          | –         | –         | –                |
| NGC 362                 | -1.15                  | -0.99 | 10.02±0.22 | –         | 8.65±0.21 | -2.90±0.21       |
| M 5 <sup>(c)</sup>      | -1.11                  | -0.90 | 9.07±0.29  | –         | 8.04±0.28 | -3.64±0.28       |
| NGC 288                 | -1.07                  | -0.85 | 9.36±0.25  | –         | 8.51±0.25 | -3.80±0.25       |
| M 107                   | -0.87                  | -0.70 | 8.94±0.34  | –         | 7.67±0.40 | -3.57±0.40       |
| NGC 6380                | -0.87                  | -0.68 | 10.37±0.22 | 9.12±0.23 | 8.75±0.22 | -3.88±0.22       |
| NGC 6342                | -0.71                  | -0.53 | 9.71±0.29  | 8.67±0.33 | 8.35±0.32 | -3.70±0.32       |
| 47 Tuc                  | -0.70                  | -0.59 | 7.88±0.19  | 6.93±0.21 | 6.69±0.19 | -3.71±0.19       |
| M 69                    | -0.68                  | -0.55 | 9.57±0.23  | –         | 8.43±0.25 | -3.51±0.25       |
| NGC 6441                | -0.68                  | -0.52 | 10.47±0.21 | 9.49±0.21 | 9.12±0.20 | -3.90±0.20       |
| NGC 6624                | -0.63                  | -0.48 | 9.30±0.32  | 8.37±0.32 | 8.08±0.31 | -3.85±0.31       |
| NGC 6440                | -0.49                  | -0.40 | 10.02±0.23 | 8.85±0.21 | 8.33±0.21 | -3.82±0.21       |
| NGC 6553                | -0.44                  | -0.36 | 8.56±0.27  | –         | 6.92±0.27 | -3.86±0.27       |
| NGC 6528                | -0.38                  | -0.31 | 9.16±0.24  | –         | 7.85±0.25 | -4.06±0.25       |

(a) RGB Tip magnitudes from Bellazzini et al. (2004).

(b) RGB Tip magnitudes refer to star 19110813 – 6001517 in the 2MASS catalog.

(c) RGB Tip magnitudes refer to star 15183604 + 0206373 in the 2MASS catalog.

star could be a long-period variable, we also consider as the possible *candidate* RGB Tip star the reddest among the brightest four stars in our photometry (the two filled circles connected by a dotted line in Fig. 4 and 5). Note that the region mapped by our observations covers the inner  $4' \times 4'$  in each cluster (see Paper I), which allows us to sample a significant fraction of the cluster light (typically  $\approx 30\%$ ). However, in order to further check that we caught the brightest RGB star, we also accurately inspect the CMD of the external regions obtained from the 2MASS catalog. Due to its poor angular resolution ( $\approx 2''$ ), the 2MASS survey is certainly not suitable to properly sample the innermost regions of GGCs, but it can be successfully used to sample the most external regions. In two cases (namely M 5 and NGC 6752) a star in the 2MASS catalog brighter than those sampled by our observations and lying along the cluster RGB ridge line has been found. Thus, for these two clusters we assumed the magnitudes of the 2MASS stars as best estimate of the RGB Tip. Note that in the case of M 5, the new estimate found here replaces the previous estimate by Valenti et al. (2004a).

Figs. 4 and 5 also report the RGB Tip determination for the dominant population of ω Cen recently obtained by Bellazzini et al. (2004). ω Cen is the most massive stellar system in the Galactic halo (its mass is  $\approx 1$  order of magnitude larger than the one of *normal clusters*), and its RGB Tip level was measured from the sharp cut-off of the RGB LF detected by applying the edge-detector filter (the so-

-called Sobel filter). In order to include this measure in our sample, we adopt the metallicity of the dominant population ( $[Fe/H]_{CG97} = -1.60$ ,  $[M/H] = -1.39$ ), the distance modulus  $((m-M)_0 = 13.70)$  and the reddening  $(E(B-V) = 0.11)$ , as done by Bellazzini et al. (2004).

The inferred best-fitting relations to the observed points (also reported in each panel of Figs. 4 and 5 with the corresponding standard deviation) are as follows:

$$M_J^{Tip} = -5.67 - 0.31[Fe/H]_{CG97} \quad (7)$$

$$M_H^{Tip} = -6.71 - 0.47[Fe/H]_{CG97} \quad (8)$$

$$M_K^{Tip} = -6.98 - 0.58[Fe/H]_{CG97} \quad (9)$$

$$M_J^{Tip} = -5.64 - 0.32[M/H] \quad (10)$$

$$M_H^{Tip} = -6.66 - 0.49[M/H] \quad (11)$$

$$M_K^{Tip} = -6.92 - 0.62[M/H] \quad (12)$$

Statistical fluctuations are the main source of uncertainty, since the upper region of the RGB is intrinsically poorly populated. Following F00, we computed the expected error on the basis of the number of stars in the brightest two magnitude bin along the RGB. For the program clusters, the  $\sigma_{stat}$  ranges from 0.03, for the most populated up to 0.32 for the least populated clusters. In order to minimize the statistical fluctuations, complementary data from 2MASS were also used and the  $\sigma_{stat}$  of our data was re-computed on the combined sample. The derived  $\sigma_{stat}$  value have been considered as representative of the main uncertainty in the

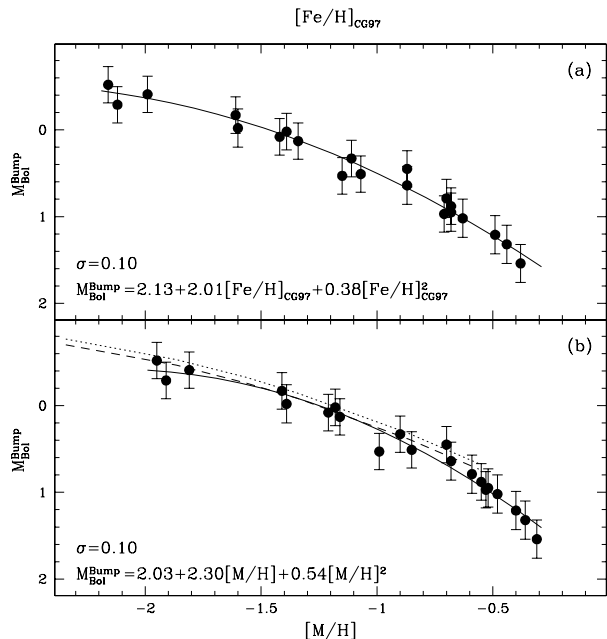


**Figure 6.** Bolometric magnitudes of the RGB Bump as a function of the cluster metallicity in both the adopted metallicity ( $[\text{Fe}/\text{H}]_{\text{CG97}}$ -panel (a) and  $[\text{M}/\text{H}]$ -panel (b)) scales. The solid lines are our best-fitting relations, the dashed line in panel (b) is the theoretical prediction by SCL97 models at  $t=12$  and  $14$  Gyr.

determination of the RGB Tip. Of course, the accuracy of the RGB Tip estimate in  $\omega$  Cen (0.16, 0.18 and 0.16 mag in J, H and K bands, respectively, see Bellazzini et al. (2004)) is by far significantly higher than that obtained in the other clusters. As can be seen from Fig. 5, our derived relations and the theoretical predictions by Cassisi et al. (2000, hereafter COO) and by SCL97 are in excellent agreement in all the three bands.

#### 4 THE THEORETICAL PLANE

Accordingly to F00, the magnitudes of the RGB Bump and Tip were transformed in the theoretical plane by using the bolometric corrections for Population II giants computed by Montegriffo et al. (1998). Fig. 6 shows the bolometric magnitudes of the RGB Bump for the program clusters. Two quadratic relations giving RGB Bump bolometric magnitude as a function of both the adopted metallicity scales have been derived:

$$M_{\text{Bol}}^{\text{Bump}} = 2.13 + 2.01[\text{Fe}/\text{H}]_{\text{CG97}} + 0.38[\text{Fe}/\text{H}]_{\text{CG97}}^2 \quad (13)$$

$$M_{\text{Bol}}^{\text{Bump}} = 2.03 + 2.30[\text{M}/\text{H}] + 0.54[\text{M}/\text{H}]^2 \quad (14)$$

The comparison between the empirical estimates and the theoretical predictions based on the SCL97 models (dashed line in panel [b] of Fig. 6), show an excellent agreement. Finally, Fig. 7 shows the bolometric magnitudes of the RGB Tip for the program clusters with varying metallicity in both the CG97 and global scales. The best-fitting relations to our data (solid line in Fig. 7) are:

$$M_{\text{Bol}}^{\text{Tip}} = -3.87 - 0.18[\text{Fe}/\text{H}]_{\text{CG97}} \quad (15)$$

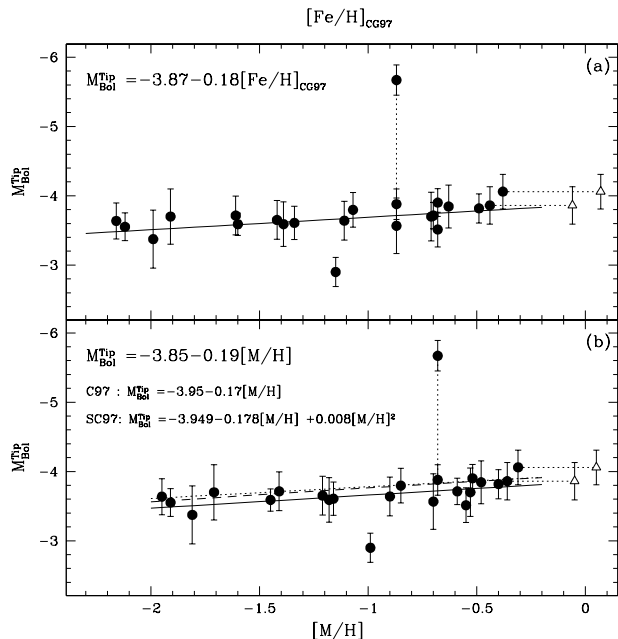


**Figure 7.** Bolometric magnitudes of the RGB Tip as a function of the cluster metallicity in both the adopted metallicity ( $[\text{Fe}/\text{H}]_{\text{CG97}}$ -panel (a) and  $[\text{M}/\text{H}]$ -panel (b)) scales. The solid lines are our best-fitting relations. Two theoretical predictions have been plotted in panel (b): Caloi et al. (1997, C97) (dotted line) and Salaris & Cassisi (1997, SC97) (dashed line).

$$M_{\text{Bol}}^{\text{Tip}} = -3.85 - 0.19[\text{M}/\text{H}] \quad (16)$$

Two theoretical relations have been overplotted in panel (b) of Fig. 7: Caloi et al. (1997) (dotted line) and Salaris & Cassisi (1997) (dashed line), respectively. Both models nicely agree with observations. As remarked by F00, the theoretical models have to be considered as an upper luminosity boundary of the observed estimates because of the statistical fluctuations affecting the observed RGB samples, intrinsically poorly populated in globular clusters (Castellani, Degl'Innocenti & Luridiana 1993).

#### 5 CONCLUSIONS

New calibrations of the RGB Bump and Tip in the J, H and K bands as well as in bolometric, based on a global sample of 24 GGCs, have been presented. The behaviour of these evolutionary features have been investigated with varying the cluster metallicity in the CG97 and global scale, thus taking into account the effect of the  $\alpha$ -enhancement.

Quadratic and linear best-fitting relations linking the RGB Bump and Tip magnitudes and metallicity, respectively, have been obtained (see eqs. 1-16). Comparisons between observations and theoretical models show a good agreement. The RGB Bump and Tip represent powerful tools to obtain independent estimates of metallicity and distance, respectively, in old stellar systems within the Local Group. The new IR adaptive optics facilities available at ground-based 8m-class telescopes as well as the future imaging capabilities of the James Webb Space Telescope are allowing to use

the RGB Tip distance indicator in galaxies well beyond the Local Group, up to a few Mpc away.

## ACKNOWLEDGMENTS

The financial support by the Agenzia Spaziale Italiana (ASI) and the Ministero dell'Istruzione, Università e Ricerca (MIUR) is kindly acknowledged. Part of the data analysis has been performed with the software developed by P. Montegriffo at the INAF-Osservatorio Astronomico di Bologna. This publication makes use of data products from the Two Micron All Sky Survey, which is a joint project of the University of Massachusetts and Infrared Processing and Analysis Center/California Institute of Technology, funded by the National Aeronautics and Space Administration and the National Science Foundation.

## REFERENCES

- Bellazzini, M., Ferraro, F. R. & Pancino, E. 2001, MNRAS, 327,15
- Bellazzini, M., Ferraro, F. R., Origlia, L., Pancino, E., Monaco, L. & Oliva, E. 2002, AJ, 124,3222
- Bellazzini, M., Ferraro, F. R., Sollima, A., Pancino, E. & Origlia, L. 2004, A&A, submitted
- Caloi, V., D'Antona, F. & Mazzitelli, I. 1997, A&A, 320, 823 (C97)
- Carretta, E. & Gratton, R. G. 1997, A&AS, 12, 95 (CG97)
- Carretta, E., Cohen, J. G. & Gratton, R. G. 2001, AJ, 122,1469
- Cassisi, S., Castellani, V., Ciarcelluti, P., Piotto, G. & Zoccali, M. 2000, MNRAS, 315,679 (C00)
- Castellani, V., Degl'Innocenti, S. & Luridiana, V. 1993, A&A, 272,558
- Cho, D. H. & Lee, S. G. 2002, AJ, 124,977
- Crocker, D. A. & Rood, R. T. 1984, in *The Observational Tests of the Stellar Evolution Theory*, ed. A. Maeder & A. Renzini (Dordrecht: Reidel), 159
- Ferraro, F. R., Messineo, Fusi Pecci, F., De Palo, M. A., Straniero, O., Chieffi, A. & Limongi, M. 1999, AJ, 118, 1738 (F99)
- Ferraro, F. R., Montegriffo, P., Origlia, L., & Fusi Pecci, F. 2000, AJ, 119, 1282, (F00)
- Fusi Pecci, F., Ferraro, F. R., Crocker, D. A., Rodd, T. R. & Buonanno, R. 1990, A&A, 238,95
- Iben, I. Jr. 1968, *Nature*, 220,143
- Monaco, L., Ferraro, F. R., Bellazzini, M. & Pancino, E. 2002, AJ, 578,50
- Montegriffo, P., Ferraro, F. R., Origlia, L. & Fusi Pecci, F. 1998, MNRAS, 297, 872
- Moorwood et al. 1992, *The Messenger*, 69,61
- Riello, M., Cassisi, S., Piotto, G., De Angeli, F., Salaris, M., Pietrinferni, A., Bono, G. & Zoccali, M. 2003, A&A, 410, 553
- Salaris, M. & Cassisi, S. 1997, MNRAS, 289, 406 (SC97)
- Savage, B. D. & Mathis, J. S. 1979, ARA&A, 17, 73
- Sollima, A., Ferraro, F. R., Origlia, L., Pancino, E. & Bellazzini, M. 2004, A&A astro-ph/0402100, in press (S04)
- Straniero, O., Chieffi, A. & Limongi, M. 1997, ApJ, 490,425 (SCL97)
- Valenti, E., Ferraro, F. R., Perina, S. & Origlia, L. 2004, A&A, astro-ph/0401153, in press
- Valenti, E., Ferraro, F. R. & Origlia, L. 2004, MNRAS, astro-ph/0403536, in press (Paper I)
- Zoccali, M., Cassisi, S., Piotto, G., Bono, G. & Salaris, M. 1999, AJ, 518, 49
- Zoccali, M. & Piotto, G. 2000, A&A, 358,943